

RESEARCH ARTICLE

10.1002/2016JC012435

Effect of tides and source location on nearshore tsunami-induced currents

Aykut Ayca¹ and Patrick J. Lynett¹¹Department of Civil and Environmental Engineering, Tsunami Research Center, University of Southern California, Los Angeles, California, USA

Key Points:

- Tsunami-induced currents can be damaging even when tsunami is small
- Effects of tide-tsunami interaction on maximum nearshore currents should be considered
- The maximum tsunami-induced currents can be well predicted by the local maximum tsunami amplitude only

Supporting Information:

- Supporting Information S1

Correspondence to:

A. Ayca,
ayca@usc.edu

Citation:

Ayca, A., and P. J. Lynett (2016), Effect of tides and source location on nearshore tsunami-induced currents, *J. Geophys. Res. Oceans*, 121, 8807–8820, doi:10.1002/2016JC012435.

Received 5 OCT 2016

Accepted 14 NOV 2016

Accepted article online 28 NOV 2016

Published online 19 DEC 2016

Abstract Here we present the results of a numerical modeling study that investigates how event-maximum tsunami-induced currents vary due to the dynamic effects of tides and wave directivity. First, analyses of tide-tsunami interaction are presented in three harbors by coupling the tsunami with the tide, and allowing the initial tsunami wave to arrive at various tidal phases. We find that tsunami-tide interaction can change the event-maximum current speed experienced in a harbor by up to 25% for the events and harbors studied, and we note that this effect is highly site-specific. Second, to evaluate the effect of wave directionality on event-maximum currents, earthquakes sources were placed throughout the Pacific, with magnitudes tuned to create the same maximum near-coast amplitude at the harbor of study. Our analysis also shows that, for the harbor and sources examined, the effect of offshore directionality and tsunami frequency content has a weak effect on the event-maximum currents experienced in the harbor. The more important dependency of event-maximum currents is the near-harbor amplitude of the wave, indicating that event-maximum currents in a harbor from a tsunami generated by a large far-field earthquake may be reasonably well predicted with only information about the predicted local maximum tsunami amplitude. This study was motivated by the hope of constructing a basis for understanding the dynamic effects of tides and wave directivity on current-based tsunami hazards in a coastal zone. The consideration of these aspects is crucial and yet challenging in the modeling of tsunami currents.

1. Introduction

Until recently, the focus of tsunami hazard studies has mostly been overland flooding, inundation, and/or damage to coastal infrastructure due to the waves. However, the latest transoceanic tsunamis have shown that, even when there is no or little inundation, the currents generated by tsunami surges can potentially cause significant damage to maritime facilities [Lynett *et al.*, 2014]. Over the past few years, the adverse nearshore effects of tsunami-induced currents from far-field sources have been reported from many locations around the world, as well as maritime communities along the U.S. West Coast [Dengler *et al.*, 2008; Wilson *et al.*, 2012, 2013]. In 2006, an earthquake ($M_w = 8.3$) occurred near the Central Kuril Islands, which was followed by a tsunami. The peak height of the tsunami that arrived at Crescent City, California, was around 1.8 m trough to peak, but it did not cause any flooding since the largest waves coincided with the low tide. Nonetheless, strong currents began with the arrival of the first waves, causing severe damage. Docks located closest to the entrance of the inner harbor, where the currents were the strongest [Dengler *et al.*, 2008], recorded the highest damage levels, with the tsunami causing \$20 million in losses [Dengler and Uslu, 2011].

Another transoceanic event, the Maule, Chile tsunami of February 2010, generated strong and damaging currents in California. Some docks were damaged in San Diego Bay near the entrance of Shelter Island, 20 docks were damaged in the Ventura Keys in Ventura Harbor, and two boats broke free from their moorings and caused minor damage in collisions with other boats and harbor infrastructure in Santa Cruz Harbor. In addition, large charter boats left the harbor prior the arrival of the tsunami and waited 6 h for reentry as strong currents made it difficult to cruise around the entrance [Wilson *et al.*, 2012].

The largest of the recent tsunamis was the 2011 Tohoku tsunami. It caused adverse effects on every maritime facility along the U.S. West Coast, ranging from interruptions of harbor operations to the complete destruction of port infrastructure. The strongest effects and most severe damage occurred in the Crescent City and Santa Cruz Harbors [Admiral *et al.*, 2013; Wilson *et al.*, 2012, 2013]. Tsunami surges created very

strong currents in Crescent City's inner harbor, which caused extreme damage or completely destroyed the docks and boats moored at the time of the tsunami.

There are several factors that can influence the variability of event-maximum tsunami-induced currents in harbors, including the tsunami's source, distance to the target area, and nearshore features. In addition, other key considerations for obtaining a detailed and accurate description of the event-maximum tsunami currents are the tide levels and their interaction with the tsunami. Only a few studies have investigated tide-tsunami interactions, with a focus on understanding their influence on the maximum wave heights, runup, and inundation limits. This has mainly been because, until recently, the context of tsunami hazards has been limited to overland flooding and inundation. An example of these previous studies is the series of numerical experiments on tsunami-tide interactions in Cook Inlet, Alaska, conducted by *Kowalik and Proshutinsky* [2010], which involved very strong tides and frequent tsunamis. They selected Anchor Point and Anchorage as their pilot study areas and found that, at Anchor Point, tsunamis are likely to be amplified by a factor of 4–6 relative to the tsunami magnitude, depending on the tide level when the tsunami arrives. In addition, at Anchorage, a tsunami could be damped by 5% or amplified by 35%, depending on the phase of the tide when the tsunami arrived. Yet, they noted that these results were very site and event specific and could not be generalized. Similarly, *Zhang et al.* [2011] investigated the dynamic effects of tides during a real event, the 1964 Alaska tsunami. Their results revealed that the tsunami-tide interaction has a considerable influence on the resulting runup and inundation. They also suggested that the inclusion of tides is important to accurately predict coastal and, especially, estuarine inundation during tsunamis.

Mofjeld et al. [2007] performed a probabilistic analysis of the effects of tides on the maximum tsunami wave heights at Seaside, Oregon. Their approach was based on an analytical analysis of linearly superimposed exponentially decaying tsunamis, and predicted the tides on the open coast at Seaside. Although their study did not include nearshore modeling, they still determined that the means, standard deviations, and probability distribution functions of the maximum tsunami heights varied with the tides at the offshore region of Seaside. Unlike the elevation-focused studies discussed above, recent studies of *Lee et al.* [2015], where they mainly focus on effects of dynamic tides on tsunami propagation, and *Shelby et al.* [2016], in which they study tide-tsunami interaction in Hudson River Estuary, also briefly investigated the effects of tide-tsunami interaction on flow velocities, but only for limited number of tide phases. Nonetheless, their results clearly reveal that large differences can be observed in maximum current speeds due to nonlinear interaction between tsunamis and tides.

In light of these previous studies, we here aim to place another missing piece of this puzzle, and explore how the dynamic effects of tides influence the event-maximum tsunami-induced currents inside harbors and bays. It is anticipated that the tidal influence on the maximum currents in a harbor or port during a tsunami could be significant when the tidal elevation and currents are similar in magnitude to those of the tsunami, and the interaction between the tides and tsunami-induced currents can be nonlinear. Therefore, an adequate demonstration of the physics of this problem has paramount importance.

While one focus of this paper is on the relevance of tides on the maximum current field, we also examine the influence of the source location of the tsunami. In their recent study, *Borrero et al.* [2015] conducted a comprehensive sensitivity analysis of tsunami current hazards as a function of the tsunami source location. They placed equivalent tsunami sources at equally spaced azimuthal directions around the Pacific Rim, and simulated each source for selected New Zealand harbors, and assessed which source was responsible for maximum currents at each grid node in modeled harbors. Their findings suggest that the tsunami currents in harbors are more sensitive than the tsunami heights to the source location. Additionally, they also inspected spectral properties of incoming tsunamis in correspondence to harbor response for one of their modeled harbors. We approach the same idea from a different perspective. Here we attempt to determine whether the source location of the tsunami plays a major role in the predicted maximum currents inside a harbor for a specific predicted local wave height, i.e., if two different sources produce the same local maximum wave height, do they also produce similar event-maximum currents? The consideration of this hypothesis arose from inspection of recent tsunami current measurements inside harbors, and the observation that often the maximum currents occurred both early in the event and near the same time as the maximum observed amplitude. These recent measurements include those in Santa Cruz, California, where currents driven by the 2010 Chile tsunami were recorded [*Lacy et al.*, 2012]. During the 2011 tsunami, far-field current data were measured in Tauranga Harbor, New Zealand [*Borrero et al.*, 2015], Port Ayora in the

Galapagos [Lynett et al., 2012], and in Hilo, Kahului, and Honolulu harbors in Hawaii [Cheung et al., 2013]. In all of these measurements, the maximum detided tsunami currents are associated with either the first, second, or third waves, and so are not likely to be a strong function of local resonance [e.g., Rabinovich, 2009], as this process should require numerous cycles to become dominant. In essence, this hypothesis is testing whether event-maximum currents are best described through an “impulsive” model, wherein the event-maximum currents are highly correlated with the event-maximum incident amplitude, or a “harmonic” model, wherein the event-maximum currents are associated with resonantly excited modes of a harbor, driven by a quasiharmonic forcing. Further motivation for testing this hypothesis is the expectation that decisions about advisories or warnings from a far-field tsunami source are based primarily on the local height predictions from National Oceanic and Atmospheric Administration (NOAA), which already take into account the open ocean propagation. This is important in issuing advisories/warnings for harbors regarding maximum expected currents, in order to take necessary mitigation measures and to continue harbor operations if possible, especially when the direct relation between the current speeds and the observed damage is considered [Lynett et al., 2014]. Here we present a foundation for understanding the dynamic effects of tides and wave directivity on current-based tsunami hazards in a coastal zone by the application of numerical simulation tools for hazard mapping purposes.

2. Modeling Approach and Methodology

In this section, we will provide information about the numerical model that we used and the methodology followed in this study.

2.1. Tsunami Hydrodynamic Model

The hydrodynamic modeling results presented here come from the application of the “method of splitting tsunami” (MOST) numerical model [Titov and Synolakis, 1995, 1998]. The MOST model has been used extensively for tsunami hazard assessments in the United States and is currently used for operational tsunami forecasting at the NOAA Pacific Marine Environmental Laboratory (PMEL). Variants of the MOST model have been in constant use for tsunami hazard assessments in California since the mid-1990s. The MOST solves the classical 2 + 1 nonlinear shallow water (NSW) equations using a finite difference scheme. More thorough information about the theoretical background and the validation of MOST was provided by Titov and Synolakis [1998]. Thus, we will not provide more technical details of the model here because of its extensive previous usage. In this study, MOST was used to propagate tsunami waves from their source to a nearshore region through nested grids. The model propagated the tsunami waves to the shore, computing the wave amplitude, velocity, and overland inundation and captures the nonlinearity of the waves as they reach shallow water. Computations were stopped at the 5 m depth contour in all the parent grids, at which depth waves were reflected back (a solid wall boundary condition was imposed). Runup and inundation computations were only performed in the innermost grid, in which a bottom friction term was included in the momentum equations. For all the simulations presented here, the Mannings “n” friction factor was 0.03.

Table 1. Grid Setup for Each of the Three Study Sites

	Lon. Range (°E)	Lat. Range (°N)	Nx	Ny	dx (arc-sec)	dt (s)
Propagation	120–292	–74–62	2581	2879	4	10
Crescent City						
Level 1	234.2592–236.3725	39.0350–41.9884	318	444	24	2.5
Level 2	235.5617–236.1183	40.5242–41.9542	168	430	12	1.5
Level 3	235.7142–235.9133	41.6284–41.8150	240	225	3	1.5
Level 4	235.7655–235.8569	41.7165–41.7829	988	718	1/3	0.25
Pillar Point Harbor						
Level 1	236.0308–238.5392	36.0200–38.9117	302	348	30	2.5
Level 2	236.7758–238.4258	36.4333–38.5333	397	505	15	1.5
Level 3	237.4396–237.5796	37.3896–37.5396	169	181	3	1.0
Level 4	237.4600–237.5500	37.4600–37.5200	973	649	1/3	0.25
San Diego Bay						
Level 1	241.0342–242.9692	32.3908–34.1509	383	353	18	2.5
Level 2	242.1475–242.9450	32.4683–33.5408	320	430	9	1.5
Level 3	242.6450–242.9142	32.5708–32.9317	324	434	3	1.0
Level 4	242.7333–242.9037	32.5845–32.7500	1842	1788	1/3	0.25

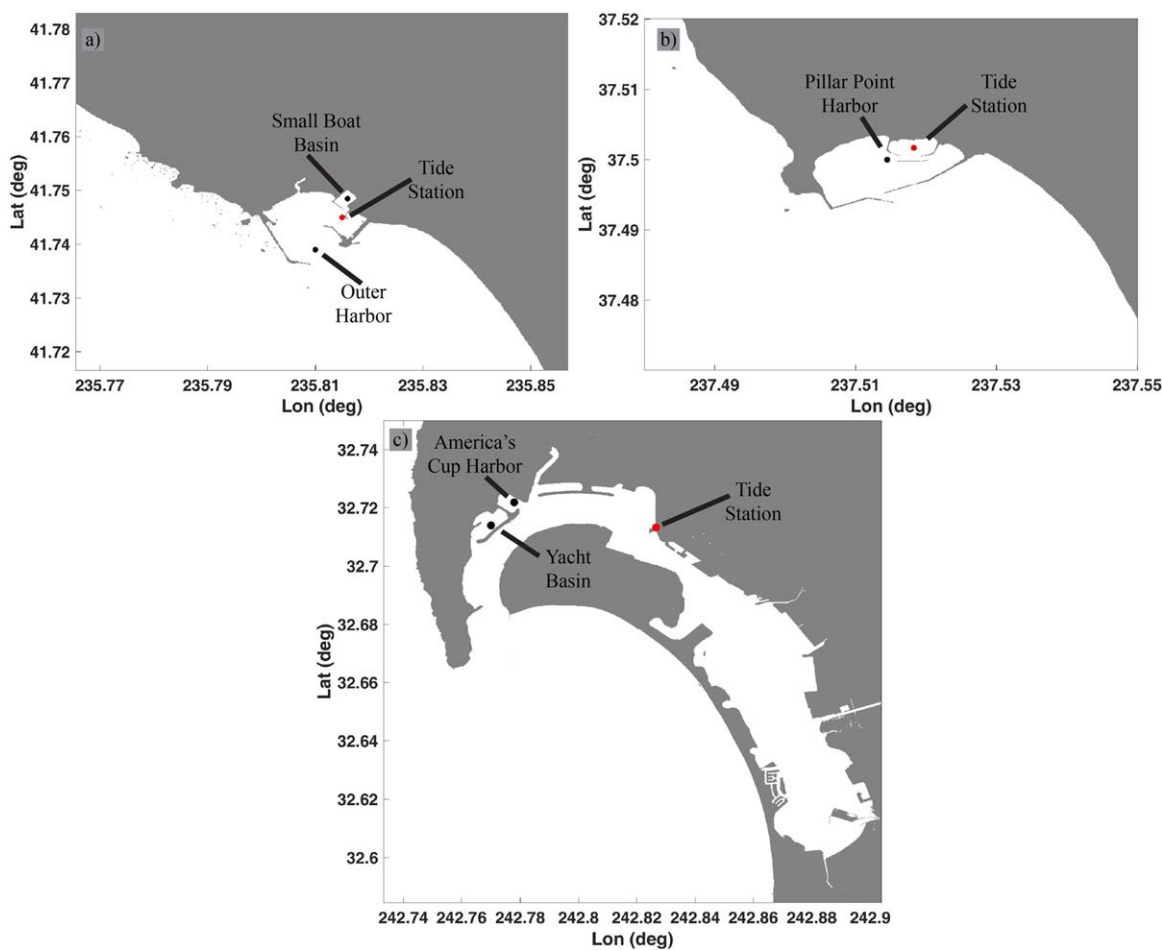


Figure 1. Layouts of the study harbors (a) Crescent City Harbor, (b) Half Moon Bay, and (c) San Diego Bay.

The outermost grid at the 4 arc min resolution covered the entire Pacific basin. Three additional grids of increasingly finer resolution were derived from data obtained from NOAA's freely available National Geophysical Data Center [ngdc.noaa.gov/mgg/inundation/tsunami/], specifically for tsunami forecasting and modeling efforts. The innermost nearshore grid with the highest resolution was at the 1/3 arc sec grid, with boundary inputs for free surface elevation and velocities from the previous MOST nested layer. Details of computational grids for all locations are listed in Table 1. Also Figure 1 maps the layout of all three-study areas in which investigated harbors and tide stations are marked with black and red dots, respectively. The detailed nested grid systems for all locations with footprints of smaller grids are shown in supporting information Figures S1 and S2.

As a final remark about the verification of the MOST results, Lynett *et al.* [2014] conducted a sensitivity analysis to understand the accuracy of MOST in resolving complex nearshore hydrodynamics, where they have compared the MOST results with a high-order fully nonlinear Boussinesq-type model (COULWAVE) and with available field data. They found out that MOST matches the tsunami amplitude phase patterns for the first several hours and the amplitude envelope for at least 24 h after the first arrival of the tsunami.

Likewise, MOST can also match the current velocities extracted from eyewitness videos. Also, on average, current velocities predicted by MOST are about 0–20% higher than COULWAVE results, which leaves MOST on the conservative side. As a

Table 2. Tide Stations Used in this Study

Station Name	Station ID	Latitude (°N)	Longitude (°W)
Crescent City	9419750	41.7450	235.8150
Pillar Point Harbor	9414131	37.5017	237.5183
San Diego Bay	9410170	32.7133	242.8267

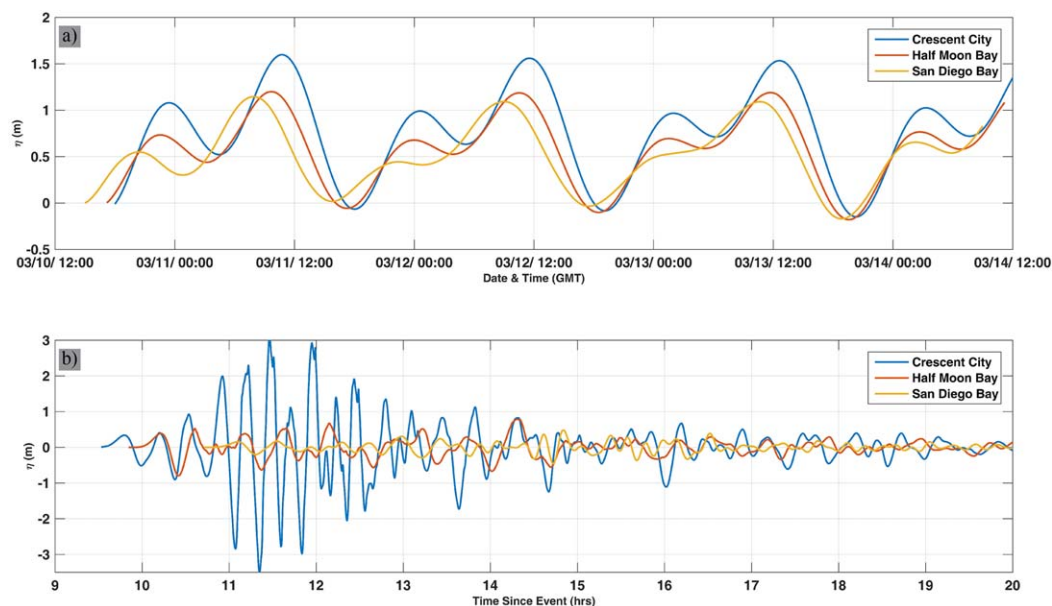


Figure 2. (a) Input time series of tides for each location extracted from tide gauge station measurement tides with respect to mean low water (MLW) level. (b) Tsunami time series from Tohoku 2011 tsunami predicted by MOST at each location. The study sites are shown in Figure 1.

result of these observations, they concluded that MOST was sufficiently capable of modeling tsunami-induced currents using a 1/3 arc sec (~10 m) grid size.

2.2. Tidal Time Series

Of particular interest in the present study was determining whether the tsunami-induced currents in ports/harbors/bays are modulated by the existing background tidal currents, and if so, what is the extent of this modulation? To answer these questions, sensitivity analysis results were compiled from selected study areas: San Diego Bay, Crescent City Harbor, and Pillar Point Harbor located inside Half Moon Bay. Several factors were taken into account when selecting these study sites. First, we wanted to examine locations in Northern, Central, and Southern California, where the tidal characteristics are modestly different. In addition, the physical characteristics of individual harbors or bays can play major roles in amplifying the effects of tides. In this regard, San Diego Bay and Pillar Point Harbor represent different types of basins. San Diego Bay is a large, long, and narrow bay, which contains different oscillatory modes, whereas Pillar Point Harbor is a small rectangular-shaped boat harbor with less complex internal hydrodynamics. Finally, in Northern California, Crescent City Harbor was a natural candidate for this study, because the most severe effects of the 2011 Tohoku tsunami were observed there. Additionally, all of the recent and past events have caused significant damage in Crescent City Harbor [Dengler *et al.*, 2008; Wilson *et al.*, 2012, 2013]. The tide data used for each study area were collected from the NOAA Tides and Currents database, where 1 min (or 6 min, depending on the type of tide station) water level data recorded during the 2011 Tohoku tsunami by local tide stations are available for download. The details about the tide stations used are listed in Table 2.

Figure 2a shows the tidal time series used in this study to force the innermost grids, which were recorded between 11 March 2011 and 15 March 2011, during the Tohoku-Oki Tsunami. The very first step in the analysis part of this work was to reproduce the tide signal numerically using MOST at the location of the tide gauge station. For this purpose, the innermost grid was only forced by tides from the boundaries, and these input files were modified and rerun until the numerically predicted tides matched the data measured at the tide gauge station. Once this was achieved, the tsunami (Figure 2b) and tidal time series (Figure 2a) obtained numerically from the

	Crescent City	Half Moon Bay	San Diego Bay
Average depth of superposition	25 m	45 m	35 m
Tide only	0.064	0.027	0.034
Tsunami only	0.129	0.018	0.014

analysis part of this work was to reproduce the tide signal numerically using MOST at the location of the tide gauge station. For this purpose, the innermost grid was only forced by tides from the boundaries, and these input files were modified and rerun until the numerically predicted tides matched the data measured at the tide gauge station. Once this was achieved, the tsunami (Figure 2b) and tidal time series (Figure 2a) obtained numerically from the

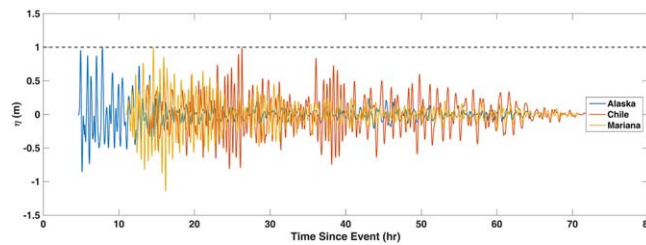


Figure 3. Time series from all three hypothetical sources predicted by model offshore Pillar Point Harbor. As can be seen, the maximum wave amplitude is 1 m for all.

MOST simulations were linearly superimposed. The linear superposition of tides and tsunamis is valid in open ocean, since their amplitudes are very small compared to the water depth [Dean and Dalrymple, 1991; Shelby et al., 2016]. However, when the linear superposition of these two waves is in the near field, like in this study, careful examination is important. The amplitude to depth ratios for tide and tsunami should be less than or close to

0.1 for linear superposition to be valid, where we are using the shallow water nonlinearity parameter as a proxy for the validity of linear superposition. In Table 3, the average depth where the tide and tsunami are combined is shown, as are amplitude-to-depth ratios in each study site. As Table 3 reveals, tides in all three sites and tsunamis in Half Moon and San Diego Bays are clearly linear at the superposition location. Only in Crescent City is the incident tsunami amplitude weakly nonlinear. Here the average depth is relatively small due to shallow areas in the northernmost part of its eastern boundary, which puts the tsunami in the weakly nonlinear regime for this part of the boundary. Nearer to the harbor entrance, the depths at the

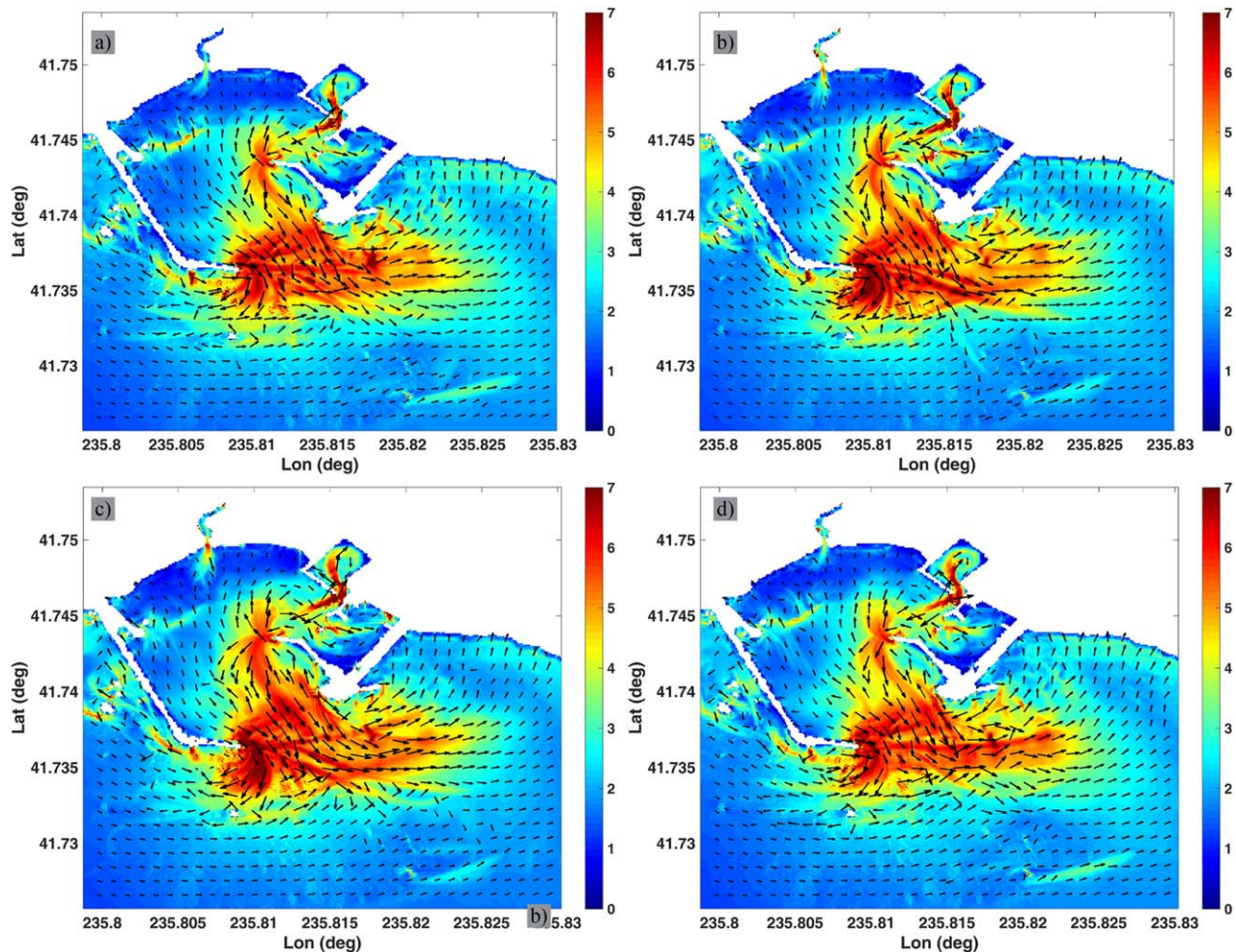


Figure 4. Maximum current speeds predicted by MOST in Crescent City for 2011 Tohoku-Oki tsunami for (a) tsunami only, (b) when tsunami arrives at midhigh tide, (c) when tsunami arrives at high tide, and (d) when tsunami arrives low tide.

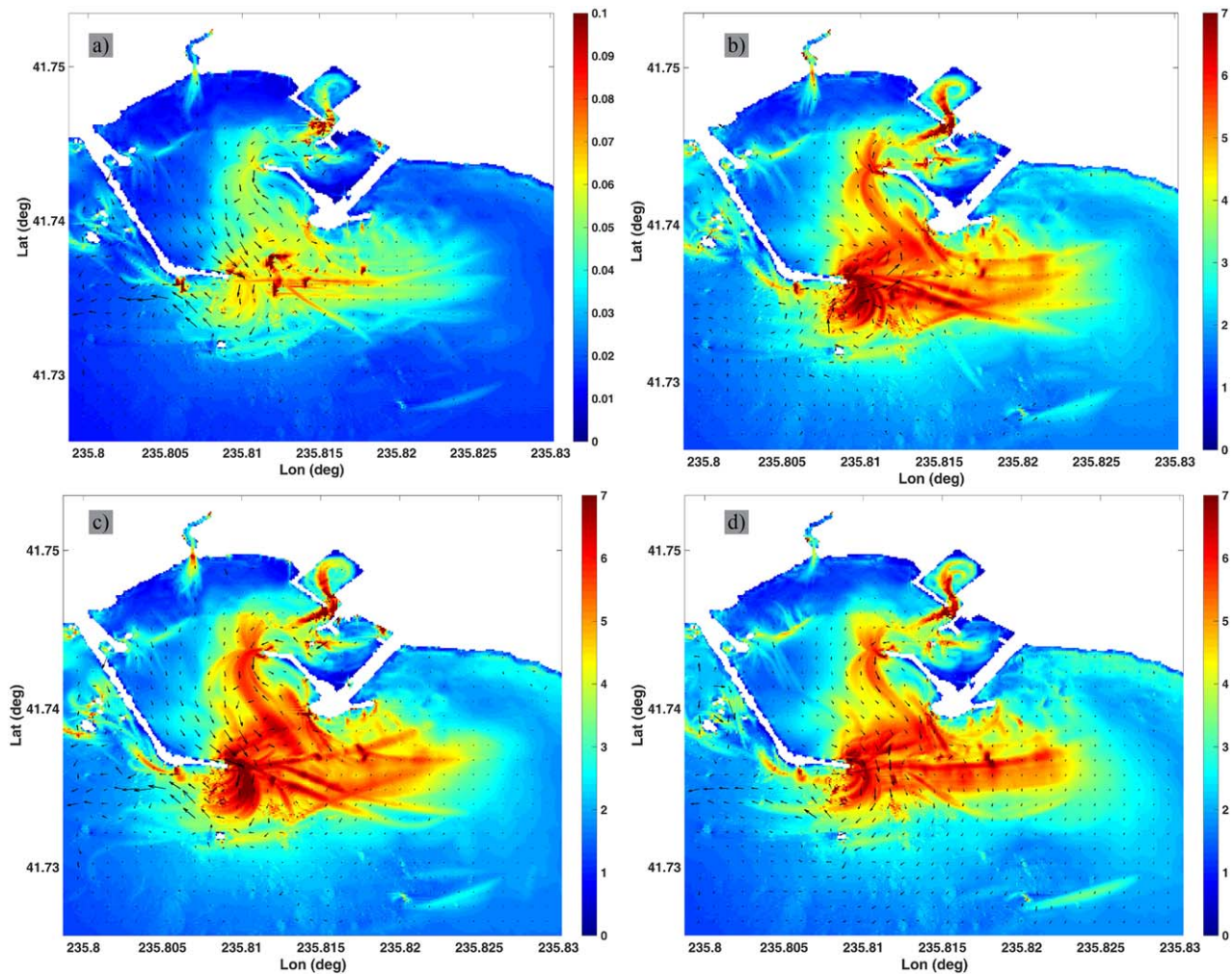


Figure 5. Maximum current speeds predicted by MOST for (a) tide only, (b) when tsunami arrives at high tide, (c) when tsunami arrives at low tide, and (d) when tsunami arrives at mid-high tide. The vectors show the direction of the tidal currents at the time of the maximum currents occur.

superposition location are greater than 50 m. Thus, we reason that the weakly nonlinear effects that might arise from a linear superposition of tide and tsunami signals offshore of the harbor entrance are small.

Here we remark that Figure 2b shows a sample time series of the tsunami recorded at one grid to illustrate the tsunami characteristics; however, MOST produces time series of free surface elevation and flow velocities at each grid node along the seaward boundaries of the innermost grids. A single tidal time series is superimposed with tsunami since the extent of the innermost grids were only a few kilometers, for which the spatial variation of tidal amplitudes will be very small. Then, the tsunami signal is shifted in time to see how the tsunami currents would have been affected if the tsunami had arrived at the maximum tide, minimum tide, or any other intermediate tide level. For each study area, tsunamis were superimposed at 12 different tide phases over a tide cycle. This illustrated the influence of the tidal currents on the event-maximum tsunami currents for various tsunami arrival times.

2.3. Wave Directionality Analysis

The approach for this analysis was to run hypothetical tsunami scenarios from three different source regions along the Pacific, and tune them in a way to ensure that they would create the same maximum offshore wave amplitude near the selected study area. Then, the resulting event-maximum current fields could be compared. Furthermore, it is well known that when examining wave-driven free surface flows, small changes (or errors) in the sea surface amplitude can lead to large changes (or errors) in the fluid speed

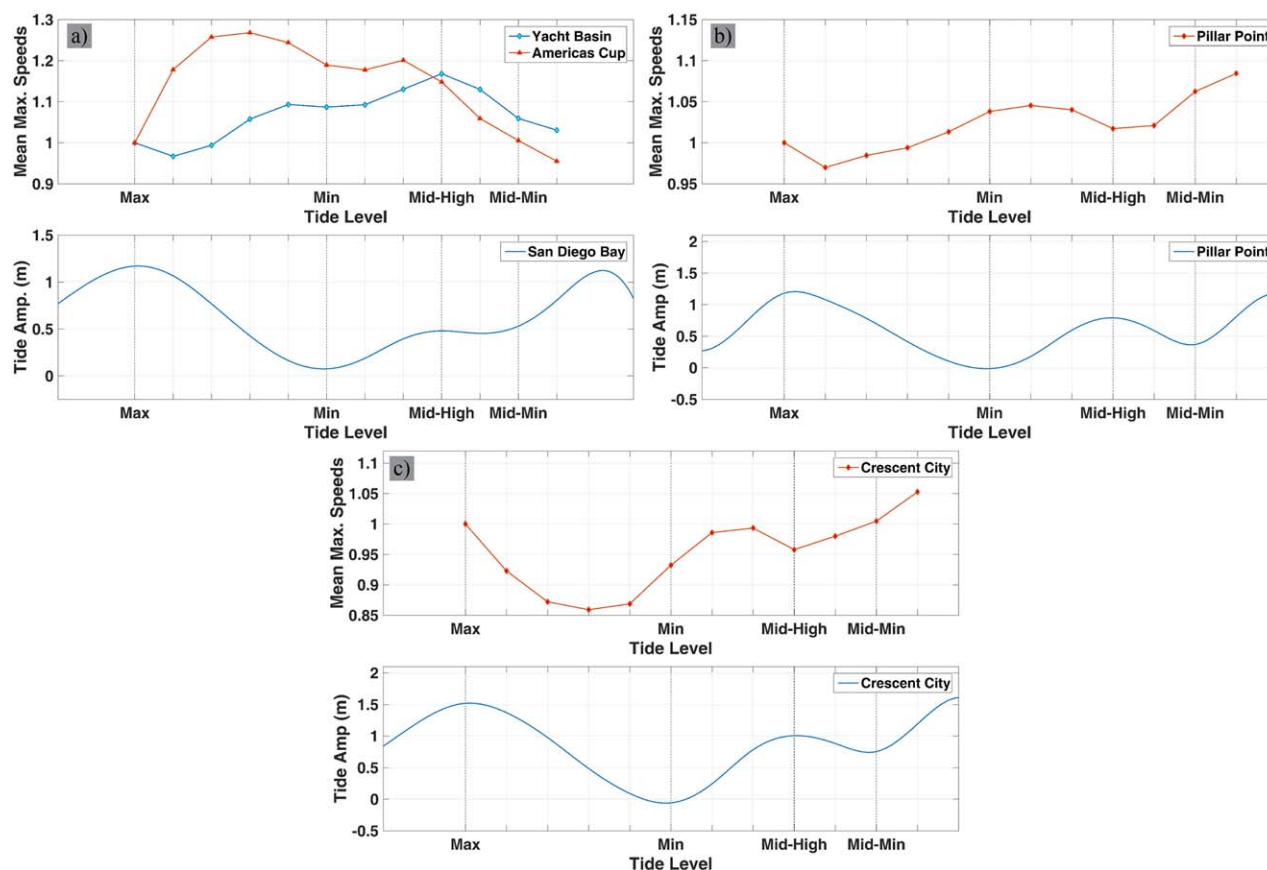


Figure 6. Upper plots show the detided normalized maximum mean currents obtained by tide + tsunami simulations plotted against tide level at (a) San Diego Bay, (b) Half Moon Bay, and (c) Crescent City Harbor.

[Lynett *et al.*, 2012; Borrero *et al.*, 2015]. Therefore, it was crucial in this study to obtain the same offshore maximum free surface elevation to within $\pm 1\%$ precision near the study area for all three sources, so that their resulting maximum current fields can be comparable.

Pillar Point Harbor, located inside Half Moon Bay, was picked as the pilot study area. Pillar Point is a south-facing harbor located along the central coast of California, and is exposed to the effects of tsunamis from all over the Pacific Rim. The harbor, with its south-facing orientation, should represent a difficult location to demonstrate that wave directionality is not an influential parameter. The sources devised for this study were assumed to arise from the Alaskan-Aleutians Subduction Zone, the Chile Subduction Zone, and the Mariana Subduction Zone. It must be noted that these sources are completely hypothetical, or, in other words they have no physical basis. We presumed these sources and tuned them to yield the maximum free surface elevation of 1 m offshore of Pillar Point Harbor. The water surface elevation time series from three different sources can be seen in Figure 3.

The model scenarios were devised by combining the NOAA-PMEL's predefined unit sources placed on fault plane segments positioned along the world's subduction zones. Each unit source is 100 km long while 50 km wide, and has 1 m displacement. Scaling and/or combining these unit sources, one can create more complex faulting scenarios. Further information about the predefined unit sources can be found in Gica *et al.* [2008].

The Alaska scenario is the combination of 12 unit sources, and represents an $M_w \sim 8.6$ earthquake with uniform slip of 3.75 m, and a rupture area of 1200 km \times 100 km in length and width, respectively. The Mariana scenario, which is an $M_w \sim 8.9$ earthquake, is 1600 km long and 100 km wide, and has 8 m of uniform slip. Lastly, the Chile scenario corresponds to an $M_w \sim 9.2$ earthquake, and 1400 km in length while 100 km in width, with the uniform slip of 23 m. Supporting information Tables S1–S3 give all the details of the source parameters used for each scenario. Due to differences in source aspect ratios and initial water depths, each of the three sources will also have modestly different energy-frequency content.

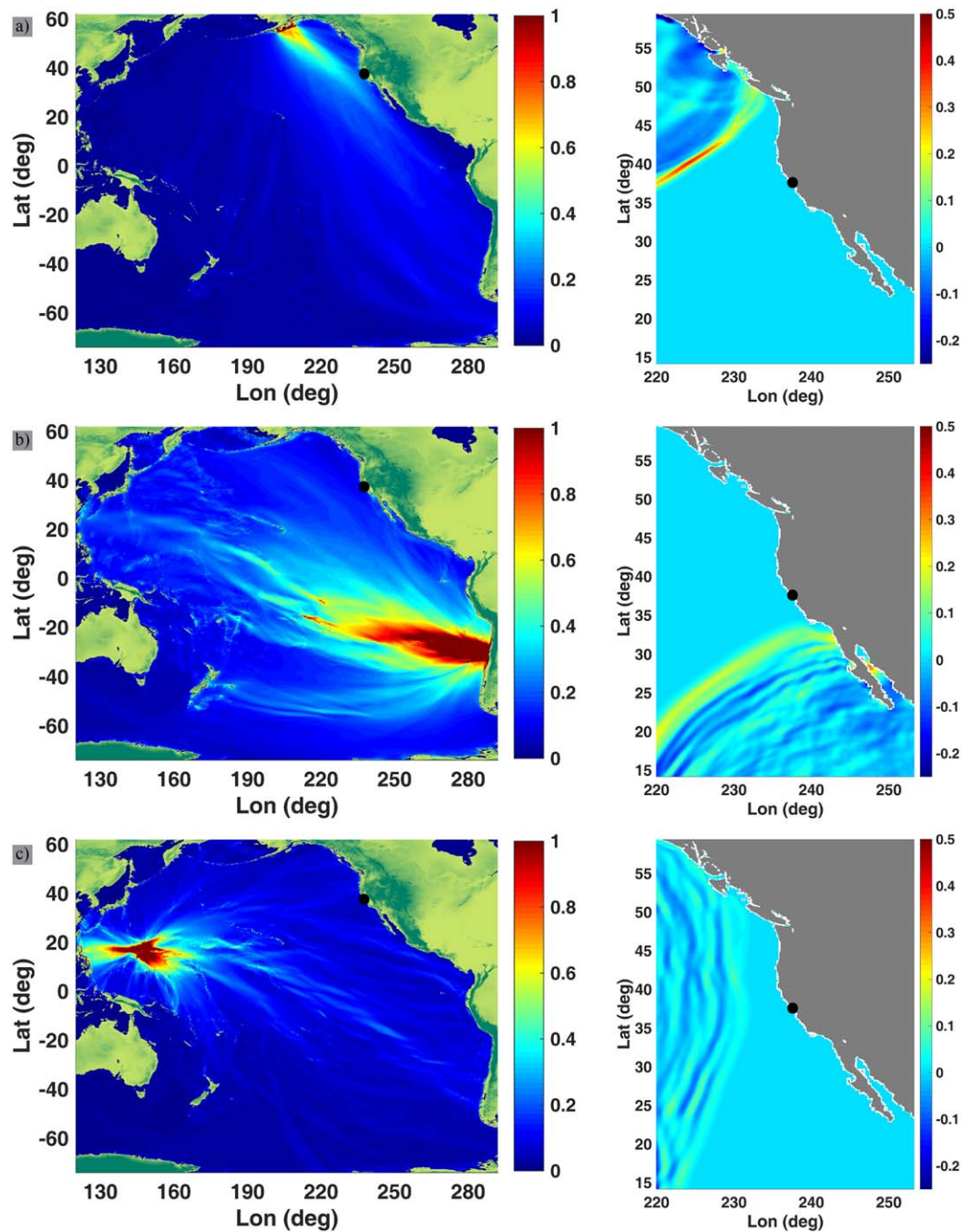


Figure 7. (left) Maximum computed tsunami heights across the Pacific and (right) the waves approaching the California from (a) Alaska, (b) Chile, and (c) Mariana scenarios. Black dots mark the location of the Half Moon Bay.

3. Model Results and Discussion

3.1. Effect of Tides on Tsunami Currents

Figures 4 and 5 show model results of the simulation-based information, which should be useful for understanding the effects of tides on event-maximum tsunami currents. When interpreting these results, the following should be kept in mind: the results presented here were detided, which means the velocity time series of the tide-only simulations were subtracted from the time series obtained from the tsunami-plus-tide simulations. This yields a time series that includes the tsunami signal and any alteration of this signal

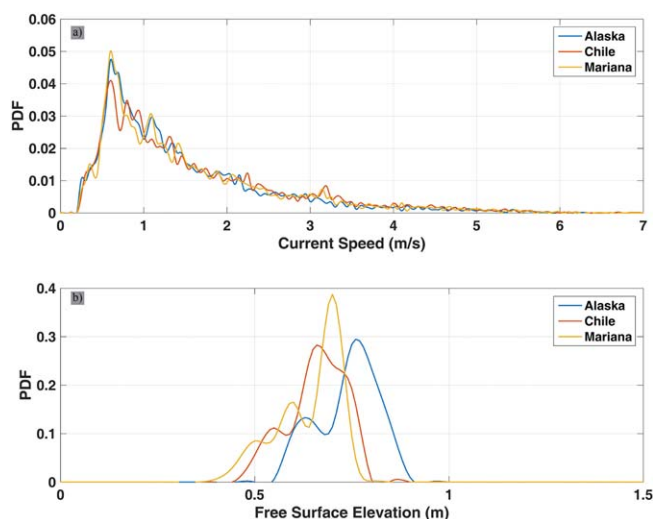


Figure 8. Probability distributions from all three sources of (a) maximum current speeds and (b) free surface elevations.

from tide-tsunami interaction. In Figure 4, we plot the maximum current speeds at Crescent City, predicted from the 2011 Tohoku tsunami source, superimposed with the tide signals for high, low, and midhigh tides, along with the results for the tsunami-only case. Although it is difficult to quantify the effects of the tides on the maximum currents from Figure 4, the differences in the overall current fields compared to the tsunami-only and various tsunami-plus-tide cases is evident.

In terms of quantification of the tide effects on event-maximum currents, we refer to Figure 6, in which the normalized means of the predicted maximum currents at each location are

plotted against the corresponding tide level. The mean of the maximum currents is the spatial average of the maximum detided currents calculated at each grid node. Subsequently, they were normalized by the mean maximum currents obtained from tsunami + max tide case. For example, the value corresponding to “Max” in Figure 6 shows the mean of the maximum currents estimated in that particular bay or harbor, if the tsunami would arrive during the high tide. The same logic applies for “Min,” “Mid-High,” “Mid-Low,” or for any other intermediate tide level. This metric makes it possible to estimate the scale of the tidal effects on tsunami currents.

Figure 6a shows a plot of the variation in the mean of the maximum speeds in San Diego Bay. We focused on two harbors: the America’s Cup Harbor located in the north, and the Yacht Basin in the south of Shelter Island, in which the strongest currents were witnessed during the 2011 Tohoku tsunami [Wilson *et al.*, 2013]. The highest modulation in the mean-maximum currents due to tides was estimated in the America’s Cup Harbor, where the difference between the lowest and highest mean-maximum currents was over 25%, with the same metric showing a 15% change in the Yacht Basin. However, these maximum tide-tsunami interaction effects in the two harbors occur at very different tidal phases, indicating that the effect is highly localized, even with two harbors in close proximity within the same bay system.

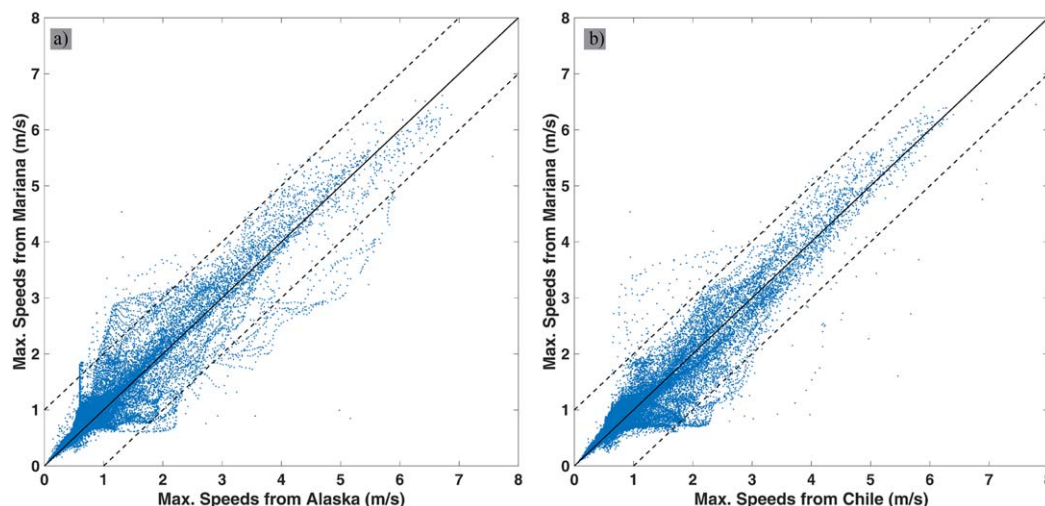


Figure 9. Scatter plot of maximum simulated current speeds as a function of water depth of all three scenarios.

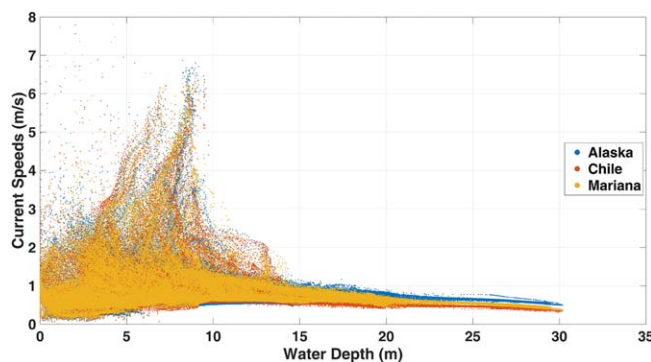


Figure 10. Maximum currents speeds of Mariana scenario versus maximum current speeds from (a) Alaska scenario and (b) Chile scenario. The solid line indicates the 1:1 relation, and two dashed lines show one standard deviation of the simulated current speeds from 1:1 relation.

tion Figure S3. Additionally, supporting information Figures S8 and S9 compare the measured water levels at tide station during Tohoku 2011 tsunami to model outputs from tsunami only, and detided tsunami + tide simulations for max., min., midhigh, and midlow tide levels.

Finally, in Pillar Point Harbor, this margin from largest to smallest is around 10%, as shown in Figure 6b, which agrees well with our a priori considerations about the scale of the tidal effects on the currents in Pillar Point. Looking across the various scaled mean-maximum speed profiles, there is no clear correlation between a specific tidal phase and the creation of the greatest currents. Thus, this comparison sheds some insight into the oft-asked question of when during the tidal cycle should one expect the tsunami currents to be greatest: it appears there is no good answer as local, site-specific effects control the response. However, what this comparison does show rather clearly is that for a tsunami with height on the order of the tidal range, the variability of tsunami arrival time with respect to the tidal phase is likely to impact the maximum currents with uncertainty in the range of $\pm 25\%$ or less.

3.2. Wave Directionality Simulations: Maximum Water Surface Elevations and Current Speeds

The results obtained in Pillar Point Harbor from the hypothetical tsunami simulations are presented in Figures 7–11. Maximum computed tsunami wave heights for the propagation grid across the Pacific, and waves propagating toward the Central California are shown in Figure 7, which gives an idea about the initial directions and wavelengths of all scenario tsunamis relative to the Half Moon Bay. It can be seen that the three sources are approaching Pillar Point Harbor from a spread of roughly 180 degrees, and thus these sources do test the limits of offshore directionality. Note, however, that while in the offshore region the wave fronts show large differences in angles of incidence, by the time these wave fronts have refracted into the shallow water offshore of the harbor, these differences are much reduced (supporting information Figure S10). It is indeed this observation that motivated this part of the study.

The probability distribution of the event-maximum speeds given in Figure 8a suggests a good agreement between all three cases. The peaks of the curves lie at around 0.7 m/s, and all three distribution shapes are similar and are characterized by slowly decaying tails at the high velocity end. On the other hand, the probability distributions of the free surface elevations display arguably more source-dependent variability, with peaks in the range of 0.6–0.8 m. However, it must be reiterated that the maximum velocity distributions contain statistically significant probability values extending beyond seven times the peak value of 0.7 m/s, while free surface elevation distributions only extend 0.5–1.0 beyond the peak. The velocity distribution for a tsunami event is expected to be much broader, in a scaled sense, than its free surface elevation distribution. This has clear implications for uncertainty quantification in tsunami speed predictions.

Taking the model data from all three scenarios, we created a scatter plot of maximum currents versus water depth as shown in Figure 9. From the figure, it is seen that the largest spread in simulated event-maximum currents exist at the depths of 5–10 m, which is due to large eddies and jets coming in and out from the outer harbor. Despite this large physical variability, the envelope of maximum currents from all scenarios shows good

In Crescent City Harbor, the difference between the smallest and largest mean-maximum currents is on the order of 20% (Figure 6c). It could be expected that greater effects from tides would be observed here, as the tidal range is larger; however, the tsunami amplitude is also larger, and these two scales compete against each other. Also, in supporting information Figures S4–S7, comparison of time series of current speeds from tide-only, tsunami only, and tide + tsunami simulations are shown, which were extracted at the synthetic gauges shown in supporting information

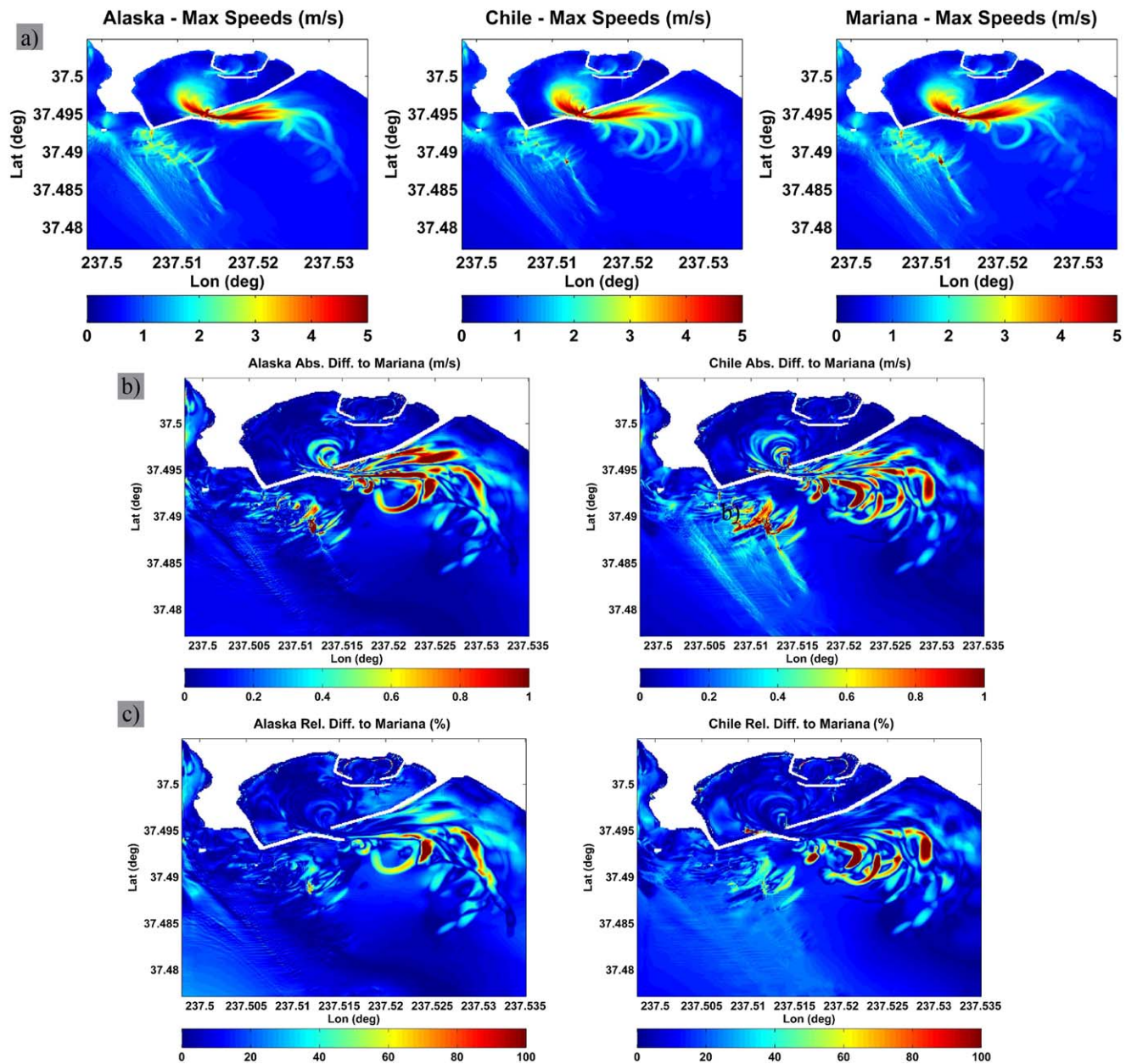


Figure 11. (a) Maximum current speeds estimated by model in Pillar Point Harbor, (b) absolute difference in maximum current speeds from Alaska and Chile cases with respect to Mariana case, and (c) relative (%) difference in maximum current speeds from Alaska and Chile cases with respect to Mariana case.

agreement. At depths greater than 15 m, the current speeds show less variability in general, and similar for all cases. The single point peaks in current speeds (speeds higher than 4 m/s) observed at depths less than 5 m are likely due to model inaccuracy at locations such as breakwater tips, sharp corners, etc. If these points are neglected (they would typically be filtered out when producing hazard maps), the maximum currents lay on the same range for this depth region as well.

The differences in the predicted event-maximum current speeds for each scenario are examined further in Figure 10. In this figure, the simulated maximum currents from the Alaska and Chile scenarios are plotted against Mariana scenario for every grid point in the computation domain. The figure reveals that the inter-scenario correlation between the maximum current speeds gets higher as the observed speed increases. For both Alaska and Chile scenarios, more than 98% of the grid points fall within ± 1 m/s of the current speeds observed in Mariana scenario, for all current speeds.

Figure 11a shows the event-maximum current speeds from all three hypothetical cases predicted by MOST. The model results suggest that high current speeds are driven by eddies formed both within and outside of the Pillar Point Harbor near the entrance, as a result of the strong advection. At the entrance to the inner harbor, however, the maxima plot shows relatively slow current speeds. Although the event-maximum current plots give an idea about the spatial variability of the current patterns, it is not easy to perceive localized scenario-based differences. To refine the local variations in the maximum speeds from different sources, Figures 11b and 11c show the absolute and relative differences in the Alaska and Chile scenarios with respect to the Mariana case. The largest deviations are observed outside of the harbor, which can be attributed to energetic eddies following different paths. Nevertheless, the error patterns inside both harbors show a great similarity. In the vicinity of the entrance of the outer harbor, the relative error is around 20% for both the Alaska and Chile scenarios where the maximum speeds occur, and 10%–15% in the inner harbor. This analysis clearly shows that, for the harbor and sources examined, the effect of offshore directionality and tsunami frequency content has a weak effect on the event-maximum currents experienced in the harbor. The much more important dependency on maximum currents is on the near-harbor amplitude of the wave, indicating that currents in a harbor from a tsunami generated by a large far-field earthquake may be reasonably predicted with only information about the predicted tsunami amplitude. Secondary effects, such as the duration or persistence of strong currents in the harbor, are likely to be driven by local harbor resonance, and thus should have a stronger source and frequency content dependence.

4. Conclusions

Observations after recent transoceanic events in California revealed that even though tsunamis from distant sources do not cause significant inundation and overland flow, they can still induce strong currents with erratic flow patterns, which can be damaging to infrastructure and vessels in ports and harbors. In this study, we conducted a sensitivity analysis focused on understanding the effects of tides and wave directionality on localized tsunami-induced currents. To this end, we addressed the fundamental question of whether the inclusion of tides in tsunami simulations has any significant impact on the tsunami-generated currents. We find that tide-induced variability in the event-maximum tsunami currents ranged from 10% to 25%, which is a variability that is, currently, lower than a typical forecast accuracy.

However, it should be kept in mind that these results do not provide a general rule in quantifying the specific tide effects on tsunami currents for a generic location. For the same tsunami event and tide signal, two neighboring harbors in San Diego Bay reacted dissimilarly. Likewise, the pattern of tide effects for Pillar Point Harbor and Crescent City Harbor also did not agree, which showed the influence of the physical characteristics of individual harbors, such as the bathymetric features or existing infrastructure, as well as the strength of the tsunami and tide signals, on these types of analyses. Therefore, to better accommodate the significance of tides in a particular area of interest in relation to tsunami currents, we strongly recommend that similar analyses be conducted and assessed on a site-specific basis, which will give the most accurate results, if a forecast accuracy better than $\pm 25\%$ is desired. Finally, we summarized our findings regarding the role of the wave source region on event-maximum tsunami currents, with the hope of determining whether decisions about maritime, current-based advisories, or warnings might be made based only on the local wave height predictions. We find that statistically the source location does not play a significant role in the prediction of event-maximum tsunami-induced currents.

Acknowledgments

The authors thank the reviewers for their constructive comments on this paper. This work was funded by grants from the California Geological Survey and the National Science Foundation. Please contact A. Ayca (ayca@usc.edu) to request the data presented here.

References

- Admire, A. R., L. A. Dengler, G. B. Crawford, B. U. Uslu, J. Borrero, S. D. Greer, and R. I. Wilson (2013), Observed and modeled currents from the Tohoku-oki, Japan and other recent tsunamis in northern California, *Pure Appl. Geophys.*, *171*, 3385–3403, doi:10.1007/s00024-014-0797-8.
- Borrero, J. C., D. G. Goring, S. D. Greer, and W. L. Power (2015), Far-field tsunami hazard in New Zealand ports, *Pure Appl. Geophys.*, *172*, 731–756, doi:10.1007/s00024-014-0987-4.
- Cheung, K. F., Y. Bai, and Y. Yamazaki (2013), Surges around the Hawaiian Islands from the 2011 Tohoku tsunami, *J. Geophys. Res. Oceans*, *118*, 5703–5719, doi:10.1002/jgrc.20413.
- Dean, R. G., and R. A. Dalrymple (1991), Water wave mechanics for engineers and scientists, in *Advanced Series on Ocean Engineering*, pp. 295–325, World Sci., Singapore.
- Dengler, L. A., and B. Uslu (2011), Effects of harbor modifications on Crescent City, California's tsunami vulnerability, *Pure Appl. Geophys.*, *168*(6–7), 1175–1195, doi:10.1007/s00024-010-0224-8.

- Dengler, L. A., B. Uslu, A. Barberopoulou, J. C. Borrero, and C. Synolakis (2008), The vulnerability of Crescent City, California, to tsunamis generated by Earthquakes in the Kuril Islands region of the Northwestern Pacific, *Seismol. Res. Lett.*, *79*(5), 608–619, doi:10.1785/gssrl.79.5.608.
- Gica, E., M. C. Spillane, V. V. Titov, C. D. Chamberlin, and J. C. Newman (2008), Development of the forecast propagation database for NOAA's Short-Term Inundation Forecast for Tsunamis (SIFT), Tech. Memo. OAR PMEL-139, 89 pp., Gov. Print. Off., Seattle, Wash.
- Kowalik, Z., and A. Proshutinsky (2010), Tsunami-tide interactions: A cook inlet case study, *Cont. Shelf Res.*, *30*(6), 633–642, doi:10.1016/j.csr.2009.10.004.
- Lacy, J. R., D. M. Rubin, and D. Buscombe (2012), Currents, drag, and sediment transport induced by a tsunami, *J. Geophys. Res.*, *117*, C09028, doi:10.1029/2012JC007954.
- Lee, H. S., T. Shimoyama, and S. Popinet (2015), Impacts of tides on tsunami propagation due to potential Nankai Trough earthquakes in the Seto Inland Sea, Japan, *J. Geophys. Res. Oceans*, *120*, 6865–6883, doi:10.1002/2015JC010995.
- Lynett, P. J., J. Borrero, R. Weiss, S. Son, D. Greer, and W. Renteria (2012), Observations and modeling of tsunami-induced currents in ports and harbors, *Earth Planet. Sci. Lett.*, *327–328*, 68–74, doi:10.1016/j.epsl.2012.02.002.
- Lynett, P. J., J. Borrero, S. Son, R. Wilson, and K. Miller (2014), Assessment of the tsunami-induced current hazard, *Geophys. Res. Lett.*, *41*, 2048–2055, doi:10.1002/2013GL058680.
- Mofjeld, H. O., F. I. González, V. V. Titov, A. J. Venturato, and J. C. Newman (2007), Effects of tides on maximum tsunami wave heights, *Nat. Hazards*, *22*(1), 71–89, doi:10.1023/A:1008198901542.
- Rabinovich, A. B. (2009), Seiches and harbor oscillations, in *Handbook of Coastal and Ocean Engineering*, edited by Y. C. Kim, pp. 193–236, World Sci., Singapore.
- Shelby, M., S. T. Grilli, and A. R. Grilli (2016), Tsunami hazard assessment in the Hudson River Estuary based on dynamic tsunami tide simulations, *Pure Appl. Geophys.*, *173*, 1–39, doi:10.1007/s00024-016-1315-y.
- Titov, V., and C. Synolakis (1995), Modeling of breaking and nonbreaking long-wave evolution and runup using VTCS-2, *J. Waterw. Port Coastal Ocean Eng.*, *121*(6), 308–316, doi:10.1061/(ASCE)0733-950X(1995)121:6(308).
- Titov, V., and C. Synolakis (1998), Numerical modeling of tidal wave run-up, *J. Waterw. Port Coastal Ocean Eng.*, *124*(4), 157–171, doi:10.1061/(ASCE)0733-950X(1998)124:4(157).
- Wilson, R., C. Davenport, and B. Jaffe (2012), Sediment scour and deposition within harbors in California (USA), caused by the March 11, 2011 Tohoku-oki Tsunami, *Sediment. Geol.*, *282*, 228–240, doi:10.1016/j.sedgeo.2012.06.001.
- Wilson, R. I., et al. (2013), Observations and impacts from the 2010 Chilean and 2011 Japanese tsunami in California (USA), *Pure Appl. Geophys.*, *170*, 1127–1147, doi:10.1007/s00024-012-0527-z.
- Zhang, Y. J., R. C. Witter, and G. R. Priest (2011), Tsunami-tide interaction in 1964 Prince William sound tsunami, *Ocean Modell.*, *40*, 246–259, doi:10.1016/j.ocemod.2011.09.005.